INTERACTION OF A LOCALIZED SHEAR ALFVÉN WAVE WITH THE ANISOTROPIC CONDUCTING IONOSPHERE: BEHAVIOUR IN A NEAR-SOURCE REGION

Shigeru FUJITA

Kakioka Magnetic Observatory, 595, Kakioka, Yasato-machi, Niihari-gun, Ibaraki 315-01

and

Tsutomu TAMAO

Geophysics Research Laboratory, University of Tokyo, 3-1, Hongo 7-chome, Bunkyo-ku, Tokyo 113

Abstract: We present results of detailed numerical analysis of effects of the nonuniform, anisotropic conducting ionosphere on the localized shear Alfvén wave, in association with the origin of pc-1 geomagnetic pulsations observed on the ground in high latitudes. Employing a simple four-layer model that consists of the evanescent magnetosphere for the fast magnetosonic wave, the ducting upper ionosphere, the *E*-layer with anisotropic conductivities, and the metallic earth, we obtain numerical solutions representing the behaviour of surface magnetic variations in a near-source region. The rate of spatial attenuation of the induced magnetic intensity at the ground varies with a horizontal distance from the center of the source, taking the same order of magnitude as that of the incident wave in the source region, but it becomes a smaller value over radial distances of an outside region. This deviation is attributed to the effects of trapped fast mode waves in the upper ionosphere, which can propagate to horizontal direction crossing vertical magnetic field lines. The major axis of polarization of the horizontal magnetic vector on the ground is nearly perpendicular to that of the incident wave, while its ellipticity and sense of rotation are almost the same as those of the incident wave.

1. Introduction

Recent network observations of pc-1 geomagnetic pulsations on the ground in high latitudes have revealed that the spatial distribution of the pulsation intensity has a concentric pattern slightly elongated in the east-west direction and the rate of apparent spatial attenuation varies from its maximum value of 10 dB/100 km near the central region to 2.5 dB/100 km in a distant region beyond 500 km from the center (HAYASHI *et al.*, 1980, 1981). They have also shown that pulsations with a left-handed polarization are frequently observed in the central region, but sometimes exhibit a tendency of variable polarization sense. These observational results are not consistent with a uniform plane wave model, and rather suggest the incidence of a localized hydromagnetic wave into the ionosphere in the source region.

In theoretical consideration of the transmission of geomagnetic pulsation signals from the magnetosphere to the surface of the earth, effects of both the anisotropic conducting ionosphere and a trough in the height distribution of the Alfvén speed in the upper ionosphere must be taken into account (JACOBS and WATANABE, 1962; MANCHESTER, 1966, 1968, 1970; CAMPBELL, 1967; C. GREIFINGER and P. GREIFINGER, 1968, 1973; P. GREIFINGER, 1972a). JACOBS and WATANABE were the first who suggested a possibility of trapping oscillations of HM-waves in the upper ionosphere as the origin of short-period pulsation. However, there has been rather a few of works in which a spatially finite extent of an incident HM-wave is essential (TAMAO, 1964; P. GREIFINGER, 1972b; INOUE, 1973; HUGHES and SOUTHWOOD, 1976a, b). TAMAO (1964) studied a case of incidence of the localized shear Alfvén wave propagating down along vertical field lines into the anisotropic conducting ionosphere, and showed that only the induced Hall current was the direct source of surface magnetic variations while the induced Pedersen current had no magnetic effect below the ionosphere. INOUE (1973) examined ionospheric effects on the spatial distribution of polarization sense of pulsations on the ground for a case of the incidence of HM-waves with the amplitude distribution localized in latitudes and propagating to the longitudinal direction. HUGHES and SOUTHWOOD (1976a, b) demonstrated the screening and modification of pulsations by the atmosphere and ionosphere, by illustrating detailed numerical results of amplitude and phase distributions of EM-fields in both altitudes and latitudes. In these studies for localized wave incidence, effects of ducted propagation in the upper ionosphere on surface magnetic signatures in a distant region from the source were excluded, because the primary motivation of these authors was not in pc-1 pulsations but in those with longer periods. GREIFINGER's paper (1972b) is the only one which includes a finite extension of the source, the ducted propagation in the upper ionosphere, as well as the transmission modification through the anisotropic conducting lower ionosphere, but numerical illustration is restricted to the frequency dependence of the amplitude of the surface magnetic field for the ducted propagation at large horizontal distances in comparison with the source size.

It is necessary to make a numerical modelling that yields detailed information useful for interpretation of observed characteristics of pc-1 pulsations at network stations in a wide range of horizontal distances. In the present paper we shall present such numerical illustrations for ionospheric effects on the localized Alfvén wave, based on a simple four-layer model including effects of both trapping of secondary waves and anisotropic conductivities.

2. Model

The incidence of a localized shear Alfvén wave into the anisotropic conducting ionosphere induces both the Pedersen and Hall currents. The Pedersen current produces the up-going Alfvén wave, propagating back along the ambient magnetic field, and the down-going magnetic toroidal mode (hereafter we call it the toroidal mode). The up-going Alfvén wave is partly reflected back at the transition altitude where the sharp increase of the Alfvén speed is taking place, and the other part is transmitted into the magnetosphere. On the other hand, the Hall current generates the

up-going fast magnetosonic wave (fast wave), as well as the down-going magnetic poloidal type perturbation (poloidal mode). The fast wave is reflected back at the transition altitude between the upper ionosphere and magnetosphere. Thus generated fast waves are important for pc-1 geomagnetic pulsations in middle and low latitudes, because they can propagate across the ambient magnetic field lines, being trapped within a trough of the Alfvén velocity distribution in the upper ionosphere. We should note here that magnetic disturbances associated with the toroidal mode in the neutral atmosphere are negligibly small in comparison with those of the poloidal mode, since the displacement current for such low-frequency waves is negligible. Thus, the magnetic disturbances observed at the ground are due to the poloidal mode, which is evanescent in altitudes in the atmosphere.

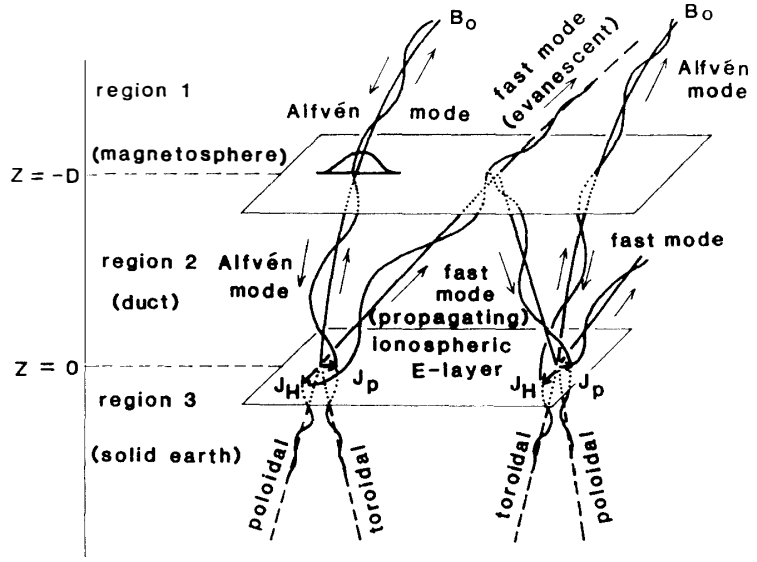

Fig. 1. A schematic illustration of the incidence of a localized shear Alfvén wave, induced Pedersen (J_P) and Hall (J_H) currents in the ionosphere, associated generation of the Alfvén and fast magnetosonic waves in the upper ionosphere and magnetosphere, as well as the poloidal and toroidal modes of magnetic disturbances in a metallic earth.

As is shown in Fig. 1, we employ here a simple four-layer model in representing the magnetosphere-ionosphere-solid earth system. In cylindrical coordinates (r, ϕ, z) where the z-axis is taken positive downward, r is the horizontal radial distance from the injection center, and the ambient, uniform magnetic field is assumed in the positive z-direction. The top layer (region 1) in Fig. 1 is corresponding to the magnetosphere with the Alfvén speed of $V_A=V_1$. The middle layer with a thickness of D (region 2) is a ducting region for trapping fast waves in the upper ionosphere with $V_A=V_2$ ($<V_1$). Both regions 1 and 2 are hydromagnetic regions. The bottom layer (region 3) represents the solid earth with the isotropic conductivity σ_G. As a transition layer from region 2 to region 3, we assume the infinitely thin ionospheric E-region ($z=0$) with height-integrated anisotropic conductivities, Σ_P (Pedersen) and Σ_H (Hall), because the effective thickness of the E-region (several tens km) is very short compared with the wavelength of pc-1 pulsations. In the above model we have neglected the

existence of the neutral atmosphere with a thickness of about 100 km, since the geometrical attenuation of the evanescent EM-perturbations in the neutral atmosphere is quite small for perturbations with the horizontal wavelength longer than 100 km. Keeping in mind the evanescent attenuation in the atmosphere, we can neglect the magnetic disturbance of the toroidal mode in the solid earth ($z>0$). However, we should still retain the electric field perturbation associated with the magnetic toroidal mode in describing boundary conditions at $z=0$.

3. Formal Representation of EM-Perturbations in Each Region

In this section we shall give formal expressions representing EM-perturbations of different wave modes in the three regions and necessary boundary conditions connecting them. As is seen blow, these perturbations are given in terms of corresponding scalar functions, Φ, Ψ, S, and T, representing the shear Alfvén, fast, poloidal, and toroidal modes, respectively. We assume the time dependence of $\exp(-i\omega t)$, but in the following we delete this dependence for simplification. In representing HM-waves in regions 1 and 2 except for the incident localized Alfvén waves, let us use notations Φ_{jk} and Ψ_{jk} where the suffix j ($j=1$ or 2) stands for one of the two regions and k ($k=u$ and d) means the upward and downward propagating waves, respectively.

(1) Region 1 (magnetosphere, $z\leq -D$)

There are three HM-waves, one is the incident localized shear Alfvén and the other are the reflected Alfvén and transmitted fast waves. For a frequency range of pc-1 pulsations the transmitted fast wave originally generated by the Hall current in the E-region is evanescent in altitudes in this region. As is derived in Appendix, EM-fields of these waves are given by the following forms:

(a) the incident Alfvén wave;

$$\begin{pmatrix} \delta E_\perp = -\nabla_\perp \Phi_i(r, \phi) \\ \delta B_\perp = (k_1/\omega)\nabla\Phi_i \times \boldsymbol{z} \end{pmatrix} \exp(ik_1 z), \tag{1}$$

where $k_1=\omega/V_1$ and $\boldsymbol{z}$ is the unit vector in the vertical downward direction.

(b) the reflected Alfvén wave;

$$\begin{pmatrix} \delta E_\perp = -\nabla_\perp \Phi_{1u}(r, \phi) \\ \delta B_\perp = -(k_1/\omega)\nabla\Phi_{1u} \times \boldsymbol{z} \end{pmatrix} \exp(-ik_1 z), \tag{2}$$

(c) the evanescent fast wave;

$$\begin{pmatrix} \delta E_\perp = i\omega\nabla\Psi_{1u}(r, \phi)\times \boldsymbol{z} \\ \delta B = \mathrm{rot}\,(\nabla\Psi_{1u}\times \boldsymbol{z}) \end{pmatrix} \exp(\rho_1 z), \tag{3}$$

where

$$\rho_1=(\lambda^2-k_1^2)^{1/2}, \tag{4}$$

and λ is a horizontal wave number in the radial direction and the suffix $\perp$ means the transverse component to the ambient magnetic field.

(2) Region 2 (ducting ionosphere, $-D<z<0$)

Both the Alfvén and fast waves are expressed in terms of the up- and down-going waves:

(a) the Alfvén waves;

$$\begin{pmatrix}\delta E_{\perp}=-\nabla\Phi_{2k}(r,\phi)\\ \delta B_{\perp}=\pm(k_2/\omega)\nabla\Phi_{2k}\times\boldsymbol{z}\end{pmatrix}\exp(\pm ik_2 z)\,, \tag{5}$$

where

$$k_2=\omega/V_2\,. \tag{6}$$

(b) the fast waves;

$$\begin{pmatrix}\delta E_{\perp}=i\omega\nabla\Psi_{2k}(r,\phi)\times\boldsymbol{z}\\ \delta B=\mathrm{rot}\,(\Psi_{2k}\times\boldsymbol{z})\end{pmatrix}\exp(\pm i\rho_2 z)\,, \tag{7}$$

where

$$\rho_2=(k_2{}^2-\lambda^2)^{1/2}\,. \tag{8}$$

In the above, we should take both $k=d$ and u, corresponding to the double signs $\pm$ in the exponent, which stand for the down- and up-going waves.

(3) Region 3 (solid earth, $z>0$)

EM-field perturbations in this region are evanescent in altitudes, so we adopt the following forms:

(a) poloidal magnetic mode;

$$\begin{pmatrix}\delta E_{\perp}=-i\omega\nabla S(r,\phi)\times\boldsymbol{z}\\ \delta B=\mathrm{rot}\,(\nabla S\times\boldsymbol{z})\end{pmatrix}\exp(-\rho_3 z)\,, \tag{9}$$

with

$$\rho_3=(\lambda^2-\kappa^2)^{1/2}\,, \tag{10}$$

$$\kappa^2=i\omega\mu_0\sigma_G+(\omega/c)^2\,, \tag{11}$$

where μ_0 and c are the free space permeability and the velocity of light.

(b) toroidal magnetic mode;

$$\begin{pmatrix}\delta E=-i\omega\ \mathrm{rot}\,(\nabla T(r,\phi)\times\boldsymbol{z})\\ \delta B_{\perp}=\mathrm{rot\ rot}\,(\nabla T\times\boldsymbol{z})\end{pmatrix}\exp(-\rho_3 z)\,. \tag{12}$$

The above form eq. (12) yields the magnetic field of the toroidal mode given by

$$\delta B_{\perp}=-\kappa^2\exp(-\rho_3 z)\nabla T(r,\phi)\times\boldsymbol{z}\,.$$

Consequently, the toroidal magnetic field is negligible in comparison with the poloidal one for $\kappa^2\ll 1$ in the neutral atmosphere wherein $\sigma_G=0$ and $\kappa^2=(\omega/c)^2$.

(4) Boundary conditions at $z=0$ and $z=-D$

At the interface ($z=-D$) between regions 1 and 2, the tangential components of both electric and magnetic fields should be continuous. The horizontal component of the electric field is also continuous in crossing the ionospheric E-region ($z=0$), but the height-integrated surface current makes a jump of the tangential magnetic fields, *i.e.*,

$$\boldsymbol{z}\times(\delta B_3-\delta B_2)=\Sigma_{\mathrm{P}}\delta E+\Sigma_{\mathrm{H}}\boldsymbol{z}\times\delta E\,. \tag{13}$$

Thus, in association with the incidence of the localized shear Alfvén wave with

the scalar potential $\Phi_i(r, \phi)$, we have eight boundary conditions by which the eight scalar functions introduced above can be represented in terms of Φ_i.

4. Incident Shear Alfvén Wave with a Localized Amplitude Distribution

As was given in the last section, the EM-field perturbations of the localized shear Alfvén wave are expressed by the scalar potential $\Phi_i(r, \phi)$. Bearing in mind the observed concentric pattern of the amplitude distribution of pc-1 pulsations in high latitudes, we now take the following form,

$$\Phi_i(r, \phi)=E_0 r_0(r/r_0)^{|m|} \exp\left[-(r/r_0)^2+im\phi\right], \tag{14}$$

where r_0 is a horizontal scale length of the source region, m is the azimuthal wave number, and the amplitude E_0 is constant. In the numerical calculation to be shown in the next section, we have employed a case of $m=-1$ which is consistent with the left-handed polarization of the horizontal magnetic vector in the central region of the injected source.

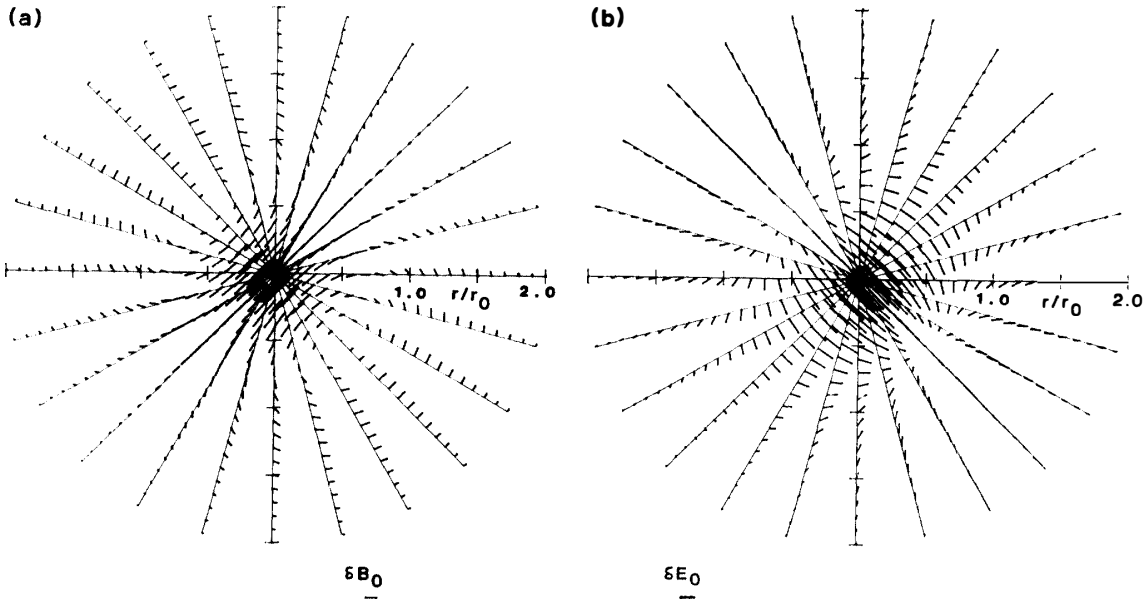

Fig. 2. Horizontal patterns of the magnetic (a) and electric (b) vectors of the incident wave for $r_0/D=0.2$, viewed from the above. In the lower corner the horizontal electric and magnetic intensities at $r=r_0$ are shown.

Pattern of the magnetic and electric field vectors on the horizontal plane, corresponding to the scalar potential Φ_i given in eq. (14) with $m=-1$ at the fixed phase, are shown in Figs. 2a and 2b, respectively. As seen in Fig. 2b, the electric field pattern has a sink and a source, which occur at the radial distance $r=r_0/2^{1/2}$ from the center. In a region surrounding the sink we have the upward field-aligned current, and there is an anticlockwise magnetic vortex viewed from the above, while in the source region the field-aligned current flows down into the ionosphere and a clockwise magnetic vortex is taking place as is seen in Fig. 2a. These patterns rotate anticlockwise as a

whole with advance in time. In the outer region beyond the radial distance $r=r_0/2^{1/2}$, the sense of polarization of horizontal vectors changes from the left-handed to the right-handed one and the amplitudes decrease considerably compared with those in the central region.

To proceed further analysis in the cylindrical coordinate we expand all of scalar functions defined in the previous section into the Fourier-Bessel integral form. For instance, the Fourier-Bessel transform of the scalar potential of the incident wave given in eq. (14) becomes

$$\tilde{\Phi}_i(\lambda, \phi)=E_0 r_0^{3/2}(r_0\lambda/2)^m \exp\left[-(r_0\lambda/2)^2+im\phi\right], \tag{15}$$

and we shall use the similar notation for others in the following.

5. Characteristics of the Surface Magnetic Disturbance

We discuss here numerical results about the surface magnetic disturbance. Employed parameters are as follows; $\mu_0 V_2 \Sigma_P=\mu_0 V_2 \Sigma_H=1(\Sigma_P=\Sigma_H\simeq 1.6$ mho), $\mu_0 V_2 D\sigma_G=1000(\sigma_G\simeq 1.6\times 10^{-3}$ mho/m), $V_2/V_1=0.4$ ($V_1=1250$ km/s), $r_0/D=0.2$ ($r_0=200$ km), and $\omega D/V_2=2$ ($\omega=1$ s^{-1}). Quantities in parentheses are typical values for $D=1000$ km and $V_2=500$ km/s.

5.1. *Spatial dependence of magnetic intensity*

In Fig. 3, spatial dependences of intensity of horizontal magnetic disturbances (Fig. 3a) on the ground and those of the incident wave in the magnetosphere (Fig. 3b) are shown. From these figures we can obtain the following characteristic features.

(1) Two curves of B_h ($=\sqrt{B_r^2+B_\phi^2}$) in Fig. 3c are similar to each other at radial distances less than $2r_0$. It is also evident that the horizontal magnetic vector on the ground deflects from that of the incident wave by 90°. This is due to the induced ionospheric Hall current. Thus, these results are consistent with those suggested by P. GREIFINGER (1972b).

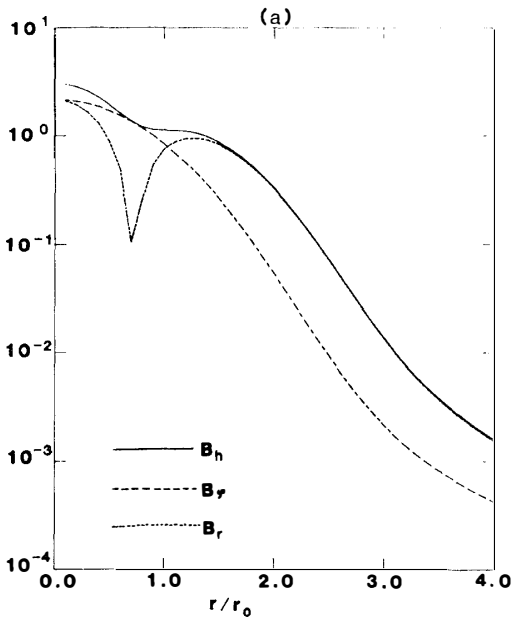

Fig. 3a.

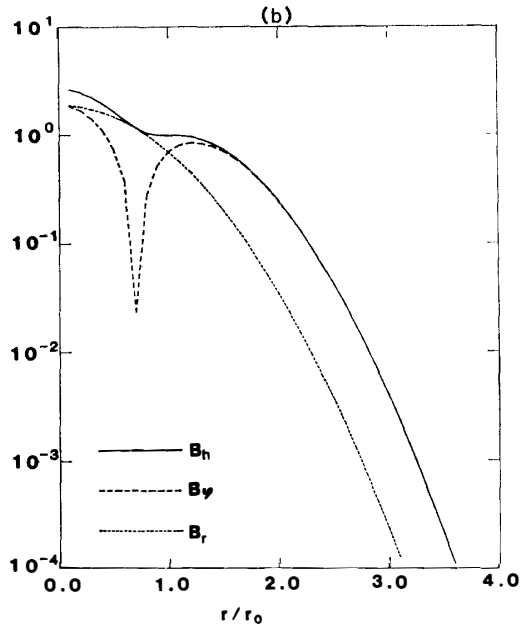

Fig. 3b.

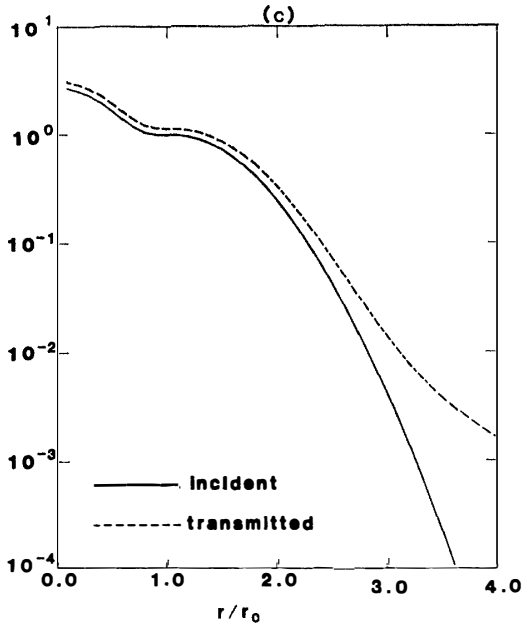

Fig. 3c.

Fig. 3. Spatial dependences of B_r (radial magnetic intensity), B_ϕ (azimuthal one), and $B_h=(B_r^2+B_\phi^2)^{1/2}$ of the transmitted disturbance on the surface of the earth (a) and those of the incident one (b). Only variations of B_h of both disturbances are exhibited in Fig. 3c. All are normalized with B_h of the incident wave at $r=r_0$.

(2) For r/r_0 being larger than 2, the spatial attenuation of the surface magnetic intensity becomes smaller than that of the incident one, since the fast mode wave generated by the ionospheric Hall current propagates radially in the ionospheric duct crossing vertical magnetic field lines.

Moreover, minima in B_ϕ of the incident wave and in B_r of the transmitted wave are taking place along a circle of $r/r_0=2^{-1/2}$ on which we have a center of a magnetic vortex of the incident wave. As will be seen later, it is also the same with the change of polarization sense.

5.2. *Spatial dependence of polarization*

As is seen in Fig. 4, the uniform ionosphere in the horizontal direction yields no effect on the polarization sense of the magnetic signature on the ground. Left-handed

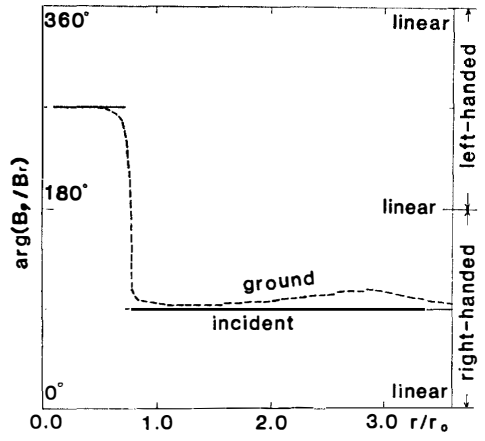

Fig. 4. Spatial dependence of the polarization sense of the horizontal magnetic vector of the incident wave and that of the transmitted one.

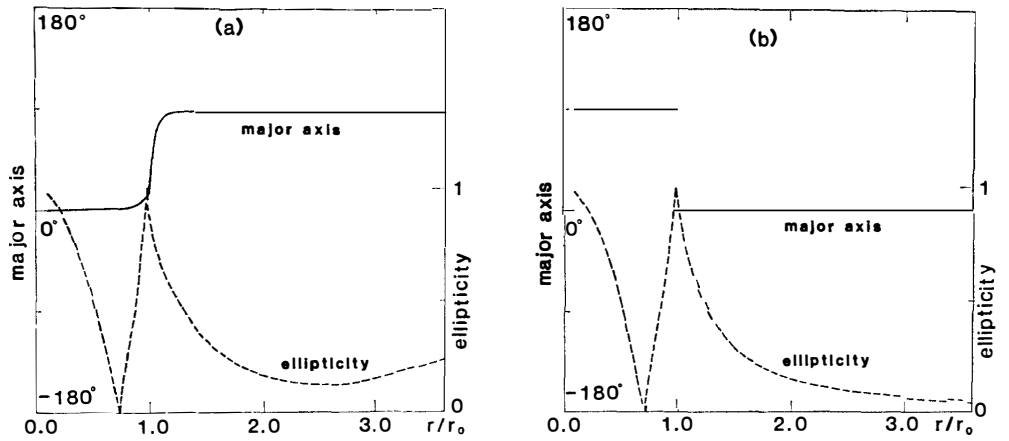

Fig. 5. A major axis direction and ellipticity of the magnetic disturbance on the ground (a), and those of the incident one (b). Angles between the major axis and the azimuthal direction are plotted for representing a direction of the major axis.

polarized magnetic disturbances are observed in a central region with $r/r_0<2^{-1/2}$, while those in an outer region beyond this radial distance are right-handed ones. This behaviour is the same as that of the incident wave. On the other hand, 90° difference in major axes between transmitted and incident magnetic disturbances is obvious in Fig. 5, although ellipticities of the both disturbances are almost the same except for the region with $r/r_0>2$. These results in the region of $r/r_0<2$ are consistent with the model of P. GREIFINGER (1972b).

In Fig. 6 we give schematic illustrations representing gross patterns of magnetic disturbances on the horizontal plane of the transmitted (Fig. 6a) and the perturbations incident (Fig. 6b). We see that the left-handed polarized disturbance is confined within the circle $r/r_0<2^{-1/2}$, and that there is a 90° difference between major axes of the transmitted and incident waves. In addition, the magnetic vector on the ground is mainly in the azimuthal direction for $r/r_0<1$ and the radial component is major one in the distant range with $r/r_0>1$. Such a tendency is also obvious in Fig. 5a.

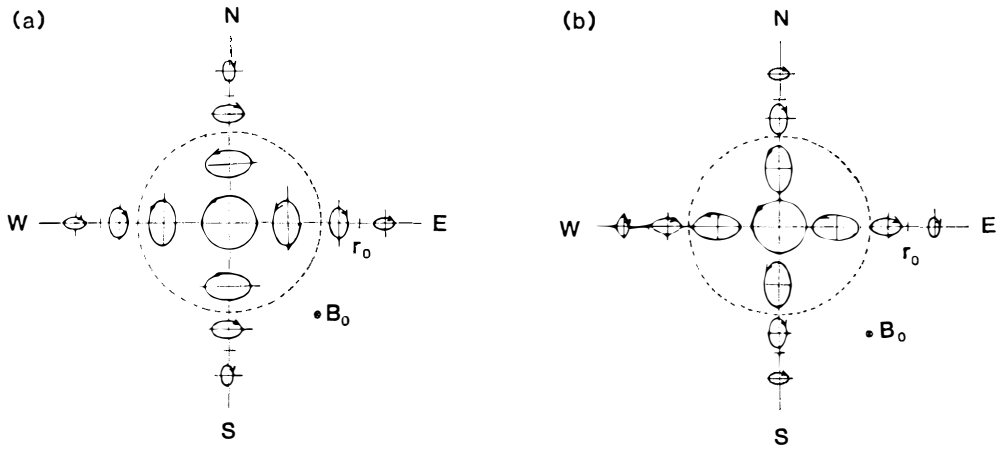

Fig. 6. Schematic illustrations of the behaviour of the surface magnetic disturbance (a), and that of the incident one (b). A left-handed polarized disturbance is confined within a circle with a dotted circle.

6. Discussion and Summary

In previous sections we have presented characteristic features of the localized injection of the shear Alfvén wave with a frequency of the pc-1 pulsation into the anisotropic conducting ionosphere. The following are main results;

(1) The incident wave is accompanied with up-going and down-going field-aligned currents.

(2) Only the poloidal magnetic disturbance can be observed on the surface of the earth.

(3) Spatial attenuations of the surface horizontal magnetic intensity and of the incident one are almost the same in the range of $r/r_0<2$. In addition, a magnetic vector rotates by 90° during transmission through the ionosphere due to the Hall current.

(4) Spatial attenuation of the surface magnetic intensity is less than that of the incident one at radial distances of $r/r_0>2$. This is attributed to the fast waves propagating in the duct in the upper ionosphere.

(5) There is the left-handed polarized magnetic disturbance in the source region where r/r_0 is less than $2^{-1/2}$, and the right-handed one in the outer region. Such a behaviour is also the same for the incident wave in the magnetosphere.

(6) The dominant surface magnetic vector is in the azimuthal direction at $r/r_0<1$ and changes to the radial direction beyond that.

Let us compare these theoretical results with the observation of pc-1 pulsations by HAYASHI *et al.* (1980, 1981).

A horizontal extent of the source is information necessary for comparison between the calculated spatial attenuation rate and the observed one. After them it has been suggested as an order of 100 km. Besides, the extent should be regarded as $2r_0$ in our model because the same spatial variations of the horizontal magnetic intensity are obtained both for the surface disturbance and the incident one in the region of $r<2r_0$. Hence, r_0 is as large as 100 km. It may be remarked here that evanescent effect of EM-disturbances in the neutral atmosphere cannot be completely neglected in the case of $r_0=100$ km. Thus, the surface disturbances are overestimated as compared with the actual one. However, since there are no trapped waves with pc-1 frequency in the atmosphere, the spatial attenuation of the surface magnetic disturbances do not change significantly when evanescent effect in the atmosphere is taken into account. Consequently, it is possible to compare the calculated results with the observational facts for the case of $r_0=100$ km.

Table 1. Attenuation rate based on the present source model.

r/r_0	Transmitted perturbation on the ground (dB/r_0)			Incident wave (dB/r_0)
Range	$r_0/D=0.1$	$=0.2$	$=0.3$	
0.1–1	9.6	9.5	9.5	9.5
1 –2	9.7	10.6	11.1	12.0
2 –3	23.4	27.7	29.3	35.8
3 –4	17.2	18.6	18.3	55.6

On the other hand, from the observation, the spatial attenuation rate near a center is about 10 dB/100 km and that at $r=500$ km is about 2.5 dB/100 km. Attenuation rates based on the present model for the case of $r_0/D=0.1$ ($r_0=100$ km for $D=1000$ km) are listed in Table 1, which shows the rate is about 20 dB/r_0 around $r=2r_0$. Those for other cases of $r_0/D=0.2$ and 0.3 are also listed in Table 1 for reference. We can see that spatial variations of the magnetic intensity against r_0 are not so much dependent on r_0. Accordingly, the spatial attenuation in the source region obtained from the present model is larger than that expected from observations, when we choose a value of $r_0/D=0.1$. We have not examined an attenuation rate at $r=500$ km, in our model, since numerical errors are significant in calculation of the surface magnetic disturbances in such a far distant region from the center. Although different results may be taken from denser network observations than that of HAYASHI *et al.*, we should employ other scalar potential of the incident wave. For example, a scalar potential presented by P. GREIFINGER (1972b) is given

$$\Phi_i(r, \phi)=E_0 r_0(r_0/r)(1-\exp(r/r_0)^2) . \tag{16}$$

Spatial attenuation rates of the magnetic disturbance of this incident wave and the associated surface magnetic disturbance obtained by numerical integrations are listed in Table 2 for the case of $r_0/D=0.1$. The maximum attenuation rate in this case is

Table 2. Attenuation rate based on Greifinger's source model ($r_0/D=0.1$).

r/r_0 Range	Incident wave (dB/r_0)	Transmitted wave on the ground (dB/r_0)
0.1–1	6.8	6.2
1 –2	6.0	5.9
2 –3	6.2	5.5
3 –4	5.0	4.7

about 6 dB/r_0 near the center, which is the same order of observational one for $r_0=$ 100 km. However, this model is not suitable for examination on effects of the ducting fast wave in the upper ionosphere, because there is no significant difference in attenuation rates between the incident wave and the transmitted one at horizontal distances with $r/r_0 \leqq 4$. Further computation is difficult due to numerical error associated with rapid oscillations of Bessel functions in the integrand.

As for the polarization, it is revealed that the ionosphere does not affect it during transmission except 90° rotation of the major axis of the polarization ellipsoid. Besides, the observation by HAYASHI *et al.* statistically shows that distribution of the left-handed polarized wave is bounded in a central region surrounded by a region of right-handed one. Therefore, the localized source model presented in this study or in the paper of P. GREIFINGER (1972b) is necessary to explain these facts, although denser network observations of pc-1 pulsations will be necessary to confirm the realistic source model.

Acknowledgements

One of the authors (S.F.) is very grateful to Dr. K. HAYASHI for his fruitful dis-

cussions on the observational facts. Gratitudes are also due to Dr. M. KAWAMURA, the former Director of Kakioka Magnetic Observatory, for his encouragement. All computations have been done with the remote batch system of the Computer Center at the Meteorological Research Institute installed at Kakioka Magnetic Observatory.

References

CAMPBELL, W. H. (1967): Low attenuation of hydromagnetic waves in the ionosphere and implied characteristics in the magnetosphere for Pc 1 events. J. Geophys. Res., **72**, 3429–3445.

GREIFINGER, C. and GREIFINGER, P. S. (1968): Theory of hydromagnetic propagation in the ionospheric waveguide. J. Geophys. Res., **73**, 7473–7490.

GREIFINGER, C. and GREIFINGER, P. S. (1973): Wave guide propagation of micropulsations out of the plane of the geomagnetic meridian. J. Geophys. Res., **78**, 4611–4618.

GREIFINGER, P. S. (1972a): Ionospheric propagation of oblique hydromagnetic plane wave at micropulsation frequencies. J. Geophys. Res., **77**, 2377–2391.

GREIFINGER, P. S. (1972b): Micropulsations from a finite source. J. Geophys. Res., **77**, 2392–2396.

HAYASHI, K., KOKUBUN, S., OGUTI, T., TSURUDA, K., MACHIDA, S., KITAMURA, T., SAKA, O., WATANABE, T. and HORITA, R. E. (1980): Profiles of Pc 1 geomagnetic pulsation based on multi-point observation in high latitudes. Highlight of the Japaneses IMS Program. Tokyo, ISAS, Univ. Tokyo, 206–214.

HAYASHI, K., KOKUBUN, S., OGUTI, T., TSURUDA, K., MACHIDA, S., KITAMURA, T., SAKA, O. and WATANABE, T. (1981): The extent of Pc 1 source region in high latitudes. Can. J. Phys., **59**, 1097–1105.

HUGHES, W. J. and SOUTHWOOD, D. J. (1976a): The screening of micropulsation signals by the atmosphere and ionosphere. J. Geophys. Res., **81**, 3234–3240.

HUGHES, W. J. and SOUTHWOOD, D. J. (1976b): An illustration of geomagnetic pulsation structure by the ionosphere. J. Geophys. Res., **81**, 3241–3247.

INOUE, Y. (1973): Wave polarizations of geomagnetic pulsations observed in high latitudes on the earth's surface. J. Geophys. Res., **78**, 2959–2976.

JACOBS, J. A. and WATANABE, T. (1962): Propagation of hydromagnetic waves in the lower exosphere and the origin of short period geomagnetic pulsations. J. Atmos. Terr. Phys., **24**, 413–434.

MANCHESTER, R. N. (1966): Propagation of Pc 1 micropulsations from high to low latitudes. J. Geophys. Res., **71**, 3749–3754.

MANCHESTER, R. N. (1968): Correction of Pc 1 micropulsations at spaced stations. J. Geophys. Res., **73**, 3549–3556.

MANCHESTER, R. N. (1970): Propagation of hydromagnetic emissions in the ionospheric duct. Planet. Space Sci., **18**, 299–307.

TAMAO, T. (1964): The structure of three-dimensional hydromagnetic waves in a uniform cold plasma. J. Geomagn. Geoelectr., **16**, 89–114.

(Received July 28, 1983; Revised manuscript received December 28, 1983)

Appendix

Hydromagnetic waves in the magnetosphere and in the duct region

In the cold uniform magnetized plasma wherein the field-aligned conductivity is assumed infinite, only the ion polarization current must be taken into consideration when the frequency of a wave is much lower than the proton gyrofrequency. In such a case, Maxwell equation is written as;

$$\text{rot}\ \delta \boldsymbol{E}_{\perp} = i\omega\delta \boldsymbol{B}_{\perp}\ , \qquad \text{(A-1)}$$

and

$$\mathrm{rot}_{\perp}\,\delta\boldsymbol{B}=-(i\omega/V_{\mathrm{A}}^{2})\delta\boldsymbol{E}_{\perp}\,. \tag{A-2}$$

Time-dependence of wave disturbance is assumed as $\exp(-i\omega t)$. The notation "$\perp$" represents component perpendicular to the ambient magnetic field.

From eqs. (A-1) and (A-2) we can obtain wave equations for the Alfvén wave and the fast wave as derived by TAMAO (1964),

$$[\partial^{2}/\partial z^{2}+(\omega/V_{\mathrm{A}})^{2}]\,\mathrm{div}\,\delta\boldsymbol{E}_{\perp}=0\,, \tag{A-3}$$

and

$$[\nabla^{2}+(\omega/V_{\mathrm{A}})^{2}]\,\mathrm{rot}_{\parallel}\,\delta\boldsymbol{E}=0\,. \tag{A-4}$$

The notation "||" represents the parallel to the ambient magnetic field.

The wave in eq. (A-3) is the Alfvén wave that transports space charge. This is consequently accompanied with the field-aligned current. On the other hand, the fast wave which satisfies eq. (A-4) is accompanied by a vortex of electric field, *i.e.*, the field-aligned component of magnetic disturbance. Other remarkable points of these waves are that the Alfvén wave has no compressional component of magnetic field, and that the fast wave has no field-aligned current.

Next, the electromagnetic disturbance of HM-waves is generally expressesed by a scalar potential Φ and a vector potential $\boldsymbol{A}$. As for the Alfvén wave, it has no compressional component of magnetic disturbance, so we have

$$\delta\boldsymbol{E}_{\perp}=-\nabla_{\perp}\Phi\,, \tag{A-5}$$

and

$$\delta\boldsymbol{B}_{\perp}=\mathrm{rot}\,(\boldsymbol{z}(i\omega)^{-1}\partial\Phi/\partial z)\,, \tag{A-6}$$

from the assumption of infinite field-aligned conductivity. $\boldsymbol{z}$ in equation (A-6) is a unit vector along the z-axis.

On the other hand, for the fast wave with a compressional component of magnetic disturbance we obtain

$$\delta\boldsymbol{E}_{\perp}=-\partial\boldsymbol{A}_{\perp}/\partial t\,, \tag{A-7}$$

and

$$\delta\boldsymbol{B}=\mathrm{rot}\,\boldsymbol{A}_{\perp}\,. \tag{A-8}$$

When we select a gauge of $\mathrm{div}\,\boldsymbol{A}_{\perp}=0$, $\boldsymbol{A}_{\perp}$ is written down as

$$\boldsymbol{A}_{\perp}=\mathrm{rot}\,[\Psi(r,\phi,z,t)\boldsymbol{z}]\,, \tag{A-9}$$

where Ψ is a scalar function.

Finally, from eqs. (A-3) and (A-5), we obtain

$$(\partial^{2}/\partial z^{2}+\omega^{2}/V_{\mathrm{A}}^{2})\Phi(r,\phi,z,t)=0\,, \tag{A-10}$$

and from eqs. (A-4) and (A-7)

$$(\nabla^{2}+\omega^{2}/V_{\mathrm{A}}^{2})\Psi(r,\phi,z,t)=0\,. \tag{A-11}$$

Then, we separate Φ and Ψ into $\phi(r,\phi)\exp(ikz-i\omega t)$ and $\Psi(r,\phi)\exp(ik'z-i\omega t)$,

respectively. We obtain the following relations from eqs. (A-10) and (A-11),

$$k=\omega/V_A\,, \quad \text{for the shear Alfvén mode,} \tag{A-12}$$

and

$$(\nabla^2{}_\perp+\lambda^2)\Psi(r,\phi)=0\,, \quad \text{for the fast mode} \tag{A-13}$$

with

$$\rho^2=k^2-\lambda^2\,. \tag{A-14}$$

Electromagnetic waves in the earth

As no space change exists in the solid earth, the vector potential is expressed by

$$\boldsymbol{A}=\mathrm{rot}\,[\boldsymbol{z}S'(r,\phi,z,t)]+\mathrm{rot}\,\mathrm{rot}\,[\boldsymbol{z}T'(r,\phi,z,t)]\,. \tag{A-15}$$

The electromagnetic disturbance represented by S' is the poloidal mode which has the magnetic disturbance perpendicular to the boundary, while the toroidal mode is derived from T'.

Equations for S' and T' can be obtained from Maxwell equations, namely,

$$(\nabla^2+\kappa^2)\begin{pmatrix} S' \\ T' \end{pmatrix}=0\,, \tag{A-16}$$

where

$$\kappa^2=i\omega\mu_0\sigma_G+(\omega/c)^2\,,$$

and σ_G is the electrical conductivity of the metallic earth.

When S' and T' are separated into two parts as is similar to Φ and Ψ, we can obtain

$$(\nabla_\perp{}^2+\lambda^2)\begin{pmatrix} S \\ T \end{pmatrix}=0\,, \tag{A-17}$$

where

$$S'(r,\phi,z,t)=S(r,\phi)\exp(\rho_3 z-i\omega t)\,, \tag{A-18}$$

$$T'(r,\phi,z,t)=T(r,\phi)\exp(\rho_3 z-i\omega t)\,, \tag{A-19}$$

and

$$\rho_3{}^2=\lambda^2-\kappa^2\,. \tag{A-20}$$